Binding Geometry and Photophysical Properties of DNA-Threading Binuclear Ruthenium Complexes

Fredrik Westerlund, Mattias P. Eng, Mikael U. Winters, and Per Lincoln*

Department of Chemical and Biological Engineering, Chalmers University of Technology, SE-41296 Gothenburg, Sweden

Received: September 8, 2006; In Final Form: October 20, 2006

The DNA binding conformation and the photophysical properties of the semiflexible binuclear ruthenium complex $[\mu\text{-bidppz(phen)}_4\text{Ru}_2]^{4+}$ (**2**) were studied with optical spectroscopy and compared to the rigid, planar homologue in syn conformation $[\mu\text{-dtpf(phen)}_4\text{Ru}_2]^{4+}$ (**3**) and the parent "light-switch" complex $[\text{Ru(phen)}_2\text{dppz}]^{2+}$ (**1**). Comparison of calculated and observed absorption bands of the bridging ligand, bidppz, confirm earlier suggestions that **2** is significantly nonplanar, both free in solution and when intercalated into poly(dAdT)$_2$, but the conclusion that the intercalated conformation is an anti rotamer is not substantiated by comparison of linear and circular dichroism spectra of **2** and **3**. The behavior of the emission quantum yield as a function of temperature is similar for the two binuclear complexes **2** and **3** in different protic solvents, and a quantitative analysis suggests that, in solution, the solvent is more strongly hydrogen bonded to the excited state of **2** than to **1**. However, the observation that for **2** the radiative rate constant increases to a value similar to **1** upon intercalation into DNA suggests that the difference between **1** and **2** in accepting hydrogen bonds is less pronounced when intercalated.

Introduction

Polypyridyl ruthenium(II) complexes have received considerable attention in the past 25 years as candidates for DNA conformational probes and anticancer drugs.[1−12] Complexes containing a dipyrido[3,2-*a*:2′,3′-*c*]phenazine (dppz) ligand, e.g., $[\text{Ru(phen)}_2\text{dppz}]^{2+}$ (**1**, phen = 1,10-phenanthroline; Figure 1), have gained extra interest due to their strong intercalative DNA binding and the "light-switch" effect: binding to DNA causes a dramatic increase in luminescence intensity (>1000 times).[4,6,13−15]

Connecting two $[\text{Ru(phen)}_2\text{dppz}]^{2+}$ moieties with a single bond yields the dimer $[\mu\text{-bidppz(phen)}_4\text{Ru}_2]^{4+}$ (**2**, bidppz = 11,-11′-bi(dipyrido[3,2-*a*:2′,3′-*c*]phenazinyl); Figure 1), which binds with very high affinity to DNA, initially not by intercalation but rather in a groove.[16] However, the nonluminescent groove-bound complexes, which associate and dissociate rapidly, slowly rearrange to another binding mode by threading one of the two bulky Ru(phen)$_2$ moieties through the DNA base stack, ending up with one ruthenium moiety in each groove and the bidppz unit residing in the center of DNA, intercalated between two base pairs.[11,17−19] The large conformational changes of DNA required for the complex to thread itself through the DNA base stack leads to extremely slow DNA binding and dissociation. The threading intercalation is, just as for **1**, associated with a strong increase in emission quantum yield, making luminescence a sensitive indicator of the threaded binding mode.

For polypyridyl ruthenium(II) complexes, luminescence takes place from a charge-separated excited state of triplet character (metal to ligand charge transfer, MLCT).[20] For **1** the dppz ligand has the lowest lying π^*-orbital, and the charge transfer is localized to the dppz moiety after excitation.[21,22] There is much evidence that the quenching mechanism in protic solvents

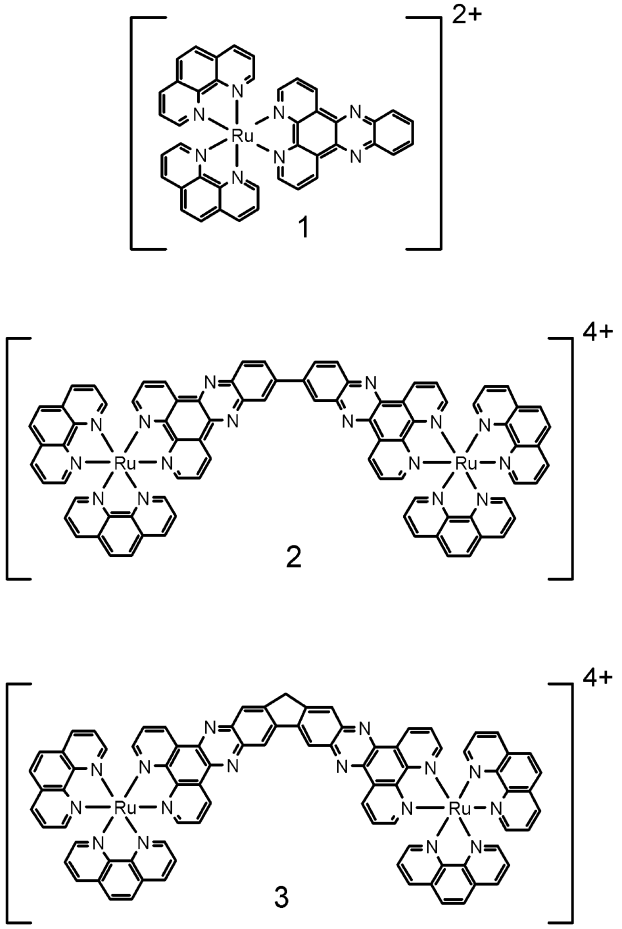

Figure 1. Structures of the ruthenium complexes in this study: $[\text{Ru(phen)}_2\text{dppz}]^{2+}$ (**1**), $[\mu\text{-bidppz(phen)}_4\text{Ru}_2]^{4+}$ (**2**), and $[\mu\text{-dtpf(phen)}_4\text{Ru}_2]^{4+}$ (**3**)

* Corresponding author. Telephone: +46-31-772 30 55. Fax: +46-31-772 38 58. E-mail: lincoln@chembio.chalmers.se.

10.1021/jp065871v CCC: $37.00
Published on Web 12/14/2006

involves hydrogen bonding to the noncoordinated aza nitrogens of the dppz ligand anion radical of the excited state. Thus, the quantum yield and the excited-state lifetime of **1** bound to DNA probe the accessibility of its phenazine moiety to water, which is found to vary a lot depending on the chirality of the ruthenium coordination and the DNA sequence.[6,23]

The photophysics of **2** is found to exhibit an even greater sensitivity to stereochemistry and DNA base composition than **1**;[17] however, structural conclusions are hampered by a lack of knowledge of the detailed photophysical properties of **2**, in particular its sensitivity to quenching by protic solvents. A further complication in the interpretation of photophysical data of **2** is the degree of conjugation in the bridging ligand, since the dihedral angle between the two dppz moieties does not necessarily need to be the same in solution as when bound to DNA. In a previous study we have interpreted linear and circular dichroism data of **2** bound to DNA as supporting a nonplanar, presumably anti, conformation, but the value of the dihedral angle remains to be determined, both free in solution and when intercalated into DNA.[17]

To assess the effect of the dihedral angle on DNA-binding geometry and photophysics, a rigid, planar homologue of the dimer [μ-dtpf(phen)$_4$Ru$_2$]$^{4+}$ (**3**, dtpf = 4,5,9,12,16,17,21,25-octaaza-23*H*-ditriphenyleno[2,3:*b*,2,3:*h*]fluorene; Figure 1), was synthesized and included in the study. Quantum mechanical calculations of ground- and excited-state energies as a function of dihedral angle were also performed at the B3LYP/6-31G(d) level for the bridging bidppz and dtpf ligands.

Recent studies of the emission from **1** in polyol solvents (glycerol, ethylene glycol, 1,2-propanediol, and 1,3-propanediol) as a function of temperature have indicated that both a short-lived non-hydrogen-bonded state and single and double hydrogen-bonded states are present during the relaxation from the excited state.[15,22] In this study a broad range of photophysical properties of the two binuclear complexes **2** and **3** is investigated and compared to **1** in polyol solvents and when bound to DNA.

Materials and Methods

Chemicals. Ethylene glycol, 1,2-propanediol, 1,3-propanediol, and glycerol were purchased from Sigma and used as obtained. Poly(dAdT)$_2$ was purchased from Amersham Biosciences and used as obtained. [Ru(phen)$_2$dppz]$^{2+}$ and [μ-bidppz(phen)$_4$Ru$_2$]$^{4+}$ were synthesized as described elsewhere.[6,17] [μ-dtpf(phen)$_4$Ru$_2$]$^{4+}$ was synthesized analogously by condensation of the appropriate enantiomer of homochiral [Ru(phen)$_2$-1,10-phenanthroline-5,6-dione](PF$_6$)$_2$ with 2,3,6,7-tetraaminofluorene. The latter was prepared by dithionite reduction of 2,7-diamino-3,6-dinitrofluorene,[24] following a slightly modified literature procedure for dinitrobenzidine reduction.[25] In contrast to the case of the synthesis of the bidppz complex, the condensation reaction of the tetraaminofluorene with the ruthenium phenanthrolinedione complex is complicated by side redox reactions. Compared to nonplanar biphenyl, the more conjugated, planar π-system of fluorene makes the corresponding tetraamine reactive enough to reduce the dtpf ligand as it is formed. Thus, only a small amount of the expected [μ-dtpf(phen)$_4$Ru$_2$]$^{4+}$ complex can be isolated directly from the reaction mixture, and instead a reduced complex is obtained. However, oxidation of the isolated crude hexafluorophosphate salt with selenium dioxide in aqueous acetonitrile proceeds smoothly to give the desired product.

2,3,6,7-Tetraaminofluorene Tetrahydrochloride. A vigorously stirred suspension of 2,7-diamino-3,6-dinitrofluorene (89 mg, 0.3 mmol[24]) in 10 mL of ethanol/water 1:1 was heated to boiling, and a total amount of 1.1 g (5.4 mmol) of sodium dithionite (technical, 85%) was added in portions over 10 min. When the red nitro compound had dissolved to a clear reddish-brown solution, the mixture was cooled on ice for 30 min. The grayish-white precipitate of amidosulfonic acids, which formed immediately on cooling, was collected on a filter and washed with water, ethanol, and diethyl ether. Boiling the precipitate for 5 min in a mixture of 1 mL of water and 1 mL of concentrated HCl hydrolyzed the sulfonyl groups and a clear yellow solution resulted, which yielded crystals of the tetrahydrochloride upon cooling. A further 1 mL of concentrated HCl was added, and the mixture was left on ice for 30 min, filtered, and washed with a little ice-cold concentrated HCl and plenty of diethyl ether to yield 65 mg (52%) of 2,3,6,7-tetraaminofluorene tetrahydrochloride as small, slightly off-white crystals.

ΛΛ-[μ-dtpf(phen)$_4$Ru$_2$]Cl$_4$ (ΛΛ-3 Chloride). Solid 2,3,6,7-tetraaminofluorene tetrahydrochloride (41 mg, 0.1 mmol) was added in portions during 10 min to a stirred solution of Λ-[Ru(phen)$_2$-1,10-phenanthroline-5,6-dione](PF$_6$)$_2$ (96 mg, 0.1 mmol[6]), sodium acetate trihydrate (61 mg, 0.45 mmol), and 10 drops of acetic acid in 4 mL of acetonitrile/water 1:1. The mixture turned from yellow brown to reddish brown. A further amount of the ruthenium complex (46 mg, 0.05 mmol) was added, and the mixture was stirred for 10 min followed by slow addition of 10 mL of 10% aqueous ammonium hexafluorophosphate solution. The black precipitate was collected on a filter and washed with plenty of water, absolute ethanol, and diethyl ether. After drying, it was dissolved in 10 mL of acetonitrile and filtered, whereupon 3 mL of a 0.1 M solution of SeO_2 in water was added. The dark blood red color of the intermediate complex changed rapidly to bright orange red. After standing for 20 min, the product was precipitated from the reaction mixture by addition of 20 mL of 10% aqueous ammonium hexafluorophosphate solution, filtered, and washed with water, ethanol, and diethyl ether. The red crystals were dissolved in 2 mL of acetonitrile and chromatographed on a 20 × 1 cm column of alumina (Brockmann activity grade III) with acetonitrile as eluent. The main orange red fraction was collected (ca. 2 mL), the chloride salt was precipitated by the addition of 0.25 g of tetrabutylammonium chloride in 5 mL of acetone, filtered, washed with acetone and diethyl ether, and dried to give 70 mg (58% based on ruthenium) of ΛΛ-**3** chloride as a red powder. Alternatively, slow addition of ammonium hexafluorophosphate in ethanol to the main fraction gave the hexafluorophosphate salt of **3**, which was collected on a filter, washed with ethanol and diethyl ether, and dried overnight at 50 °C.

UV−vis [**3**-PF$_6$ in 10% aqueous ethanol, λ_{max}/nm (ϵ/1000 M^{-1} cm^{-1})]: 435 (93), 356 (40), 319 (92), 263 (183), 222 (144).

Circular dichroism (CD) [ΛΛ-**3**-PF$_6$ in 10% aqueous ethanol, λ_{extr}/nm ($\Delta\epsilon$/M^{-1} cm^{-1})]: 467 (+42), 422 (−21), 298 (+176), 267 (+576), 256 (−271), 215 (−108).

^{1}H NMR (ΛΛ-**2**-Cl in DMSO-d_6, 400 MHz): δ 9.67 (m, 4H), 9.20 (s, 2H), 8.98 (d, 2H), 8.82 (m, 8H), 8.75 (d, 2H), 8.42 (s, 8H), 8.31 (m, 4H), 8.22 (m, 4H), 8.09 (d, 4H), 7.98 (m, 4H), 7.84 (m, 8H).

^{1}H NMR (ΛΛ-**3**-Cl in DMSO-d_6, 400 MHz): δ 9.66 (m, 4H), 9.59 (s, 2H), 8.84 (m, 10H), 8.43 (s, 8H), 8.31 (d, 4H), 8.22 (m, 4H), 8.09 (d, 4H), 7.98 (m, 4H), 7.86 (m, 8H), 4.90 (s, 2H).

The ΔΔ-enantiomer was prepared analogously from Δ-[Ru(phen)$_2$-1,10-phenanthroline-5,6-dione](PF$_6$)$_2$.

Sample Preparation. DNA samples were prepared by mixing ruthenium complex dissolved in MQ water with 2 equiv of poly(dAdT)$_2$ dissolved in buffer (150 mM NaCl, 1 mM cacodylate).

The sample concentrations for the absorption and linear dichroism and circular dichroism measurements were 3.75 μM Ru complex and 60 μM poly(dAdT)$_2$. Polyol samples were prepared by dissolving the ruthenium complexes in the different solvents. Unless otherwise stated, the absorbance in the sample was set to 0.8 at 433 nm. Concentrations were determined on a Varian Cary 4B spectrophotometer.

Absorption. Absorption measurements were performed on a Varian Cary 4B spectrophotometer. Measurements were performed in MQ water: immediately after addition of poly(dAdT)$_2$ in buffer, after 1 h at 50 °C, and after being kept at 50 °C for 16 h.

Linear dichroism (LD)[26] is defined as the difference in absorbance of linearly polarized light, parallel and perpendicular to a macroscopic orientation axis (here the flow direction):

$$\mathrm{LD} = A_{\parallel} - A_{\perp}$$

The LD spectrum is a weighted sum of the differently polarized absorption envelopes $\epsilon_i(\lambda)$ such that the isotropic absorption spectrum is

$$A_{\mathrm{iso}}(\lambda) = \sum \epsilon_i(\lambda)$$

and the linear dichroism spectrum is

$$\mathrm{LD}(\lambda) = S\sum w_i \epsilon_i(\lambda)$$

where S is the global orientation factor $0 \leq S \leq 1$, which here measures how well the helix axis of DNA is aligned in the flow field. The weights w_i depend on the angle α_i between the transition moment i and the helix axis:[7]

$$w_i = 1.5S(3\cos^2 \alpha_i - 1)$$

Samples with ruthenium complex and poly(dAdT)$_2$ in buffer were kept at 50 °C for 16 h. LD spectra were measured with a Jasco J-720 CD spectropolarimeter, equipped with an Oxley prism to obtain linearly polarized light, on samples oriented in a Couette flow cell with an outer rotating cylinder at a shear gradient of 3000 s^{-1}. All spectra were recorded at 25 °C between 220 and 650 nm and baseline-corrected by subtracting the spectrum recorded for the nonoriented sample.

Circular Dichroism. Circular dichroism (CD) is defined as the difference in absorbance of left and right circularly polarized light. CD spectra were measured on a Jasco J-720 spectropolarimeter using a 5 mm quartz cell. All spectra were performed at 25 °C and recorded between 220 and 650 nm and corrected for background contribution by subtracting the spectrum recorded for buffer only.

Steady-State Luminescence. Emission spectra were recorded on a xenon lamp equipped SPEX Fluorolog τ-3 Spectrofluorimeter (JY Horiba) using the T-channel. The samples were excited at 433 nm, and emission was measured between 500 and 850 nm. The inner filter effect due to excitation light absorption was kept low, by using a short optical path length for the excitation light. Low-temperature measurements were performed using a temperature-controlled liquid nitrogen cryostat (Oxford LN$_2$). Polyol solutions were degassed by purging with argon for 15 min, whereas the DNA experiments where performed on aereated samples.

Dissociation experiments were performed by studying the decrease in emission from the complexes leaving DNA after adding sodium dodecyl sulfate (SDS) to a final concentration of 0.5% w/w to samples with 3.75 μM ruthenium complex and 60 μM poly(dAdT)$_2$ that had been kept at 50 °C overnight. Dissociation measurements were performed on a Varian Cary Eclipse spectrofluorimeter.

Transient Emission Measurements. Measurements of the long emission lifetimes (>25 ns) were performed on a setup where the exciting light is provided by a pulsed Nd:YAG laser (Continuum Surelite II-10, pulse width <7 ns) pumping an OPO (optical parametric oscillator) giving a tunable excitation wavelength of 400−700 nm. The emitted light was collected at an angle of 90° relative to the excitation light and, after passing a monochromator, detected by a five-stage Hamamatsu R928 photomultiplier tube. The decays were collected and averaged by a 200 MHz digital oscilloscope (Tektronix TDS2200 2Gs/s) and stored by a LabView program (developed at the department), which controls the instrument setup. The oscilloscope is triggered by a photodiode that detects the exciting laser pulse. In the experiments an excitation wavelength of 440 nm was used and the emission decays were probed at 620 nm. In general, 16 measurements were averaged for each sample. The energy of the exciting laser was kept below 20 mJ/pulse to prevent photodegradation of the samples.

Short fluorescence lifetimes (<25 ns) were determined using time-correlated single photon counting. The samples were excited by the frequency-doubled output from a mode-locked Ti:sapphire laser (Tsunami, Spectra Physics), and a pulse selector (Model 3980, Spectra Physics) was used to achieve repetition rates between 0.4 and 4 MHz. The emission was collected by a microchannel plate photomultiplier tube (R3809U-50, Hamamatsu) and fed into a multichannel analyzer with 4096 channels yielding a time resolution of about 10 ps (fwhm). A minimum of 10 000 counts were recorded in the top channel, and the resulting intensity data were subsequently fitted to an exponential expression by iterative reconvolution to the instrument response and a least-squares minimization procedure with the software package FluoFit 4.0 Pro (PicoQuant).

Quantum Chemical Calculations. Quantum chemical calculations were performed using the Gaussian 03 program suite[27] at the B3LYP/6-31G(d) level. All optimizations were performed without symmetry constraints, and the resulting geometries were used for time-dependent density functional (TD-DFT) calculations of the vertical $S_n \leftarrow S_0$ excitation energies. For the rigid dtpf ligand this was only done for the fully optimized geometry, but for the flexible bidppz ligand, since a distribution of conformations is expected, the potential energy as a function of rotation was first calculated. To this end the dihedral angle between the two dppz units was varied between 0° and 180° in 10° increments and the molecule was geometry optimized with respect to all other parameters at each point. This procedure helped to determine what conformations would be most probable, or interesting in other aspects, and TD-DFT calculations were done for these conformations. The potential energy as a function of rotation was also calculated for the anion radical, a state that is involved in the approximate description of the excited state of the corresponding binuclear ruthenium complex.

Results

Table 1 compares the observed absorption maxima of [μ-bidppz(phen)$_4$Ru$_2$]$^{4+}$ (**2**) and [μ-dtpf(phen)$_4$Ru$_2$]$^{4+}$ (**3**) in water, with transition energies calculated using TD-DFT for the bridging ligands, dtpf and bidppz. For the latter calculations were made at a dihedral angle between the two dppz moieties of 0° (syn), 45°, 135°, and 180° (anti). For the rigid **3**, the calculation is in fair agreement with experiment, predicting transition energies to be only 600 cm^{-1} too high. Assuming

TABLE 1: Calculated Wavelength (λ) and Oscillator Strength (f) for the Strong Transitions in the Bridging Ligands of 2 and 3

molecule	ω^a	λ (nm)/f	λ (nm)/f	λ (nm)/f
2	0	426/0.60	317/1.39	307/0.27
2	45	399/0.48	301/1.47	291/0.06
2	135	398/0.56	301/1.18	301/0.40
2	180	410/0.98	312/0.37	309/1.03
2	exptl[b]	408/0.74[c]	312/1.08[c]	
3	0	424/0.96	310/1.10	304/0.31
3	exptl[b]	435/0.93[c]	319/0.92[c]	

[a] The dihedral angle between the two subunits of the bridging ligand of **2**. [b] Experimental data (see Material and Methods and ref 17) for the corresponding complexes are included for comparison. [c] Molar absorbance/10000.

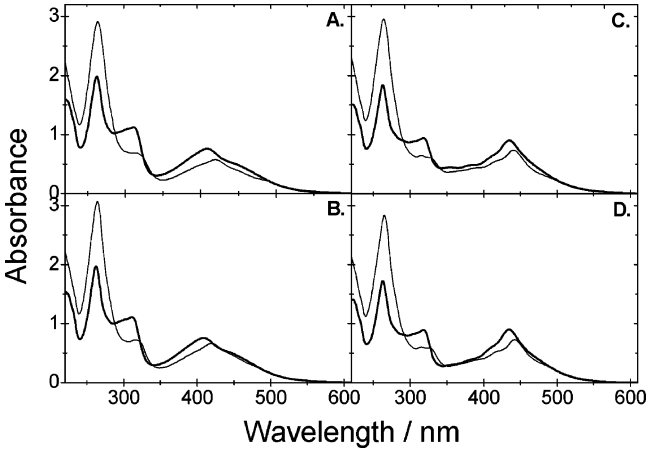

Figure 2. Absorbance spectra for ΔΔ-**2** (A), ΛΛ-**2** (B), ΔΔ-**3** (C), and ΛΛ-**3** (D). Spectra recorded in MQ water (thick) and after 1 h with poly(dAdT)$_2$ at 50 °C (thin). Measurements performed at 25 °C.

the same discrepancy for bidppz, the experimental wavelength of 408 nm for **2** would correspond to a calculated wavelength of 398 nm, very close to what is predicted for a dihedral angle of 45° or 135°.

Calculations of energy as a function of dihedral angle show that there are, for both bidppz and its anion radical, two minima with similar energies, at approximately 40° and 140° (Supporting Information, Figure S1). The calculations thus predict **2** to be nonplanar, both in the ground state and in the lowest excited MLCT state, and that it is likely to exist in aqueous solution as a 1:1 mixture of syn and anti rotamers.

Similar to the intercalating complex **1**, the binuclear complexes **2** and **3** exhibit a red shift and a hypochromic effect in the visible part of the absorption spectrum after incubation with poly(dAdT)$_2$ (Figure 2, Table 2). Whereas the red shift and hypochromicity are roughly comparable for the ΛΛ-enantiomers of the binuclear complexes, ΔΔ-**2** shows, compared to ΔΔ-**3**, a significantly larger red shift (5 nm) that seems to suggest a conformational change to a more planar, better conjugated, conformation. However, 5 nm is far from the red shifts of 27 nm (syn) and 11 nm (anti) predicted from the calculations for the planar conformations of **2**. A planar anti conformation would be expected to counteract the hypochromic effect by an increase in the absorption intensity of the unperturbed chromophore; instead, the hypochromic effect for ΔΔ-**2** is stronger than that for ΔΔ-**3** (25% compared to 16%).

The chiral ruthenium complexes **2** and **3** show very similar, strong circular dichroism (CD) in aqueous solution, both in the region of the $\pi-\pi^*$ transitions of the phenanthroline ligands around 260 nm and in the MLCT band around 450 nm

TABLE 2: Red Shift and Hypochromicity of 1, 2, and 3 upon Binding to Poly(dAdT)$_2$

molecule	$\Delta\lambda^a$ (nm)	H^b (%)
Δ-**1**[c]	9	29
Λ-**1**[c]	9	28
ΔΔ-**2**	11	25
ΛΛ-**2**	9	14
ΔΔ-**3**	6	16
ΛΛ-**3**	7	19

[a] Change in wavelength of maximum absorption in the MLCT band ($\Delta\lambda$) in poly(dAdT)$_2$ compared to water. [b] Hypochromicity (H) is calculated as the difference in absorption at λ_{max} in water and when bound to poly(dAdT)$_2$ divided by the absorption in water. The absorption when bound to DNA is from a sample heated to 50 °C for 1 h. [c] Values from the literature.[7]

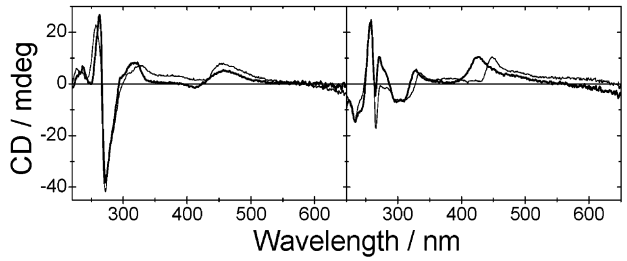

Figure 3. Difference in CD spectra for ΔΔ-enantiomers (left) and ΛΛ-enantiomers (right) of **2** (thick) and **3** (thin) calculated as CD(DNA-bound) − CD(water).

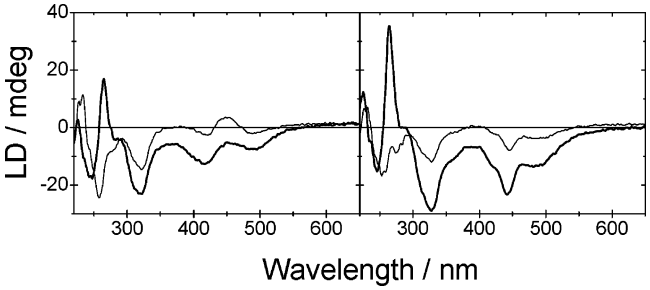

Figure 4. LD spectra of ΔΔ (thick) and ΛΛ (thin) **2** (left) and **3** (right) bound to poly(dAdT)$_2$ in its equilibrated binding mode. Measurements performed at 25 °C in 100 mM NaCl buffer.

(Supporting Information, Figure S2). The differential CD spectra ([DNA-bound] − [free]) for the four compounds, after incubation overnight with poly(dAdT)$_2$ at 50 °C, are shown in Figure 3. Interestingly, the changes induced by binding to DNA are largest at the positions of the strong $\pi-\pi^*$ transitions of the bridging ligands (around 320 and 420 nm) and are surprisingly similar when comparing the flexible **2** and the rigid, planar **3**. This indicates that the induced CD for both complexes originates mainly from oscillator coupling between electronic transitions of the DNA bases and the $\pi-\pi^*$ transitions of the bridging ligand, and that the CD that could be expected from a chiral, skewed bidppz chromophore in **2** is not strong enough to be discerned with certainty.

LD spectra of the ΔΔ- and ΛΛ-enantiomers of **2** and **3** when bound to flow-oriented poly(dAdT)$_2$ are shown in Figure 4. For all compounds, strong negative LD bands from the $\pi-\pi^*$ transitions of the bridging ligands, observed around 320 and 420 nm, suggest that their long axes are oriented roughly perpendicularly to the DNA helix axis, in support of an intercalative binding. However, the pronounced difference in the LD spectra of the enantiomers of both complexes below 300 nm, in the region of strong $\pi-\pi^*$ transitions of the phenanthroline ligands, shows that the binding geometry of ΔΔ

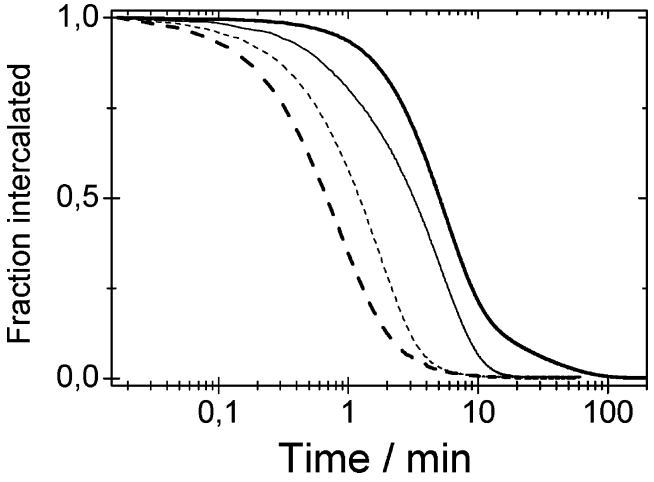

Figure 5. Dissociation from poly(dAdT)$_2$ for ΔΔ-**2** (thick solid), ΛΛ-**2** (thin solid), ΔΔ-**3** (thick dashed), and ΛΛ-**3** (thin dashed). Measurements performed at 50 °C in 100 mM NaCl buffer.

and ΛΛ differs with respect to the angle between the phenanthroline ligands and the DNA helix axis, for both **2** and **3**.[17] In particular, the molecular plane of the dtpf ligand cannot be oriented coplanar with the bases for both enantiomers of **3**, as in an idealized intercalative binding to B-DNA, since that would have resulted in LD spectra of identical shape.[7] The larger difference in the LD amplitudes of the enantiomers of **3**, compared to **2**, show further that the more rigid complex has a stronger diastereomeric differentiation with regard to binding geometry and/or DNA orientation.

The emission increases with roughly similar rates for the corresponding enantiomers of **2** and **3** when mixed with poly(dAdT)$_2$ in buffer at 50 °C, the ΛΛ-enantiomers being somewhat faster than the ΔΔ-enantiomers (data not shown). However, ΔΔ-**3** does not show the subsequent slow increase in emission characteristic of ΔΔ-**2** binding to poly(dAdT)$_2$, which is associated with shuffling of the initial distribution of threaded complexes.[19] Figure 5 shows the rate of dissociation for **2** and **3** from poly(dAdT)$_2$ at 50 °C as the change in emission intensity with time when sodium dodecyl sulfate (SDS) micelles are added. The slowness of the dissociation further supports threading intercalation for **3**.

In Table 3 emission quantum yields and lifetimes of **2** and **3** bound to poly(dAdT)$_2$ are compared with those of **1**.[6,17] For all three complexes, long lifetimes (>500 ns) are present for the Δ-enantiomers only, the enantiomer that also has the highest quantum yield. Interestingly, ΔΔ-**2** has a much higher emission quantum yield than ΔΔ-**3**. The natural lifetime (the inverse of the radiative rate constant for luminescence) falls within the range found in polyol solvents for **1** and **3** (see below); however, for both enantiomers of **2**, it is found to be significantly shorter.

Figure 6 shows the emission quantum yield between 150 and 410 K for **2** in 1,2-propanediol compared in turn to **1** in 1,2-propanediol (Figure 6A), **2** in ethylene glycol (Figure 6B), and **3** in 1,2-propanediol (Figure 6C). The emission of **3** was not studied above 50 °C since it was not stable in polyol solvent at elevated temperatures. However, **2** and **3** show almost identical behavior between 10 and 50 °C, when the emission quantum yield (emission intensity integrated between 12 000 and 18 000 cm^{-1}) is plotted against temperature in glycerol, ethylene glycol, 1,2-propanediol, and 1,3-propanediol (Supporting Information, Figure S3). The quantum yield curves (Figure 6) for all three complexes can be divided into four phases as the temperature is raised:[15,28] At low temperatures (below the glassing temperature of the solvent) the emission quantum yield is large and essentially temperature independent. In the next phase, the emission intensity decreases with temperature as a result of decreased solvent viscosity, increasing the rate of formation of strong interactions, in particular hydrogen bonds, between the complexes and the solvent. The third phase is characterized by an increase in emission intensity with increasing temperature where a local maximum is reached, suggesting that the thermodynamic equilibrium for strong solvent interactions is shifted to the left.[22] At even higher temperatures (phase 4) the emission decreases with temperature, with a slope similar to that for the parent chromophore $[Ru(phen)_3]^{2+}$.[15] In 1,2-propanediol the high-temperature maximum is shifted about 50 °C toward higher temperature for **2** compared to **1**. For both binuclear complexes the change in emission with temperature is very similar at all temperatures studied, though the quantum yield in 1,2-propanediol glass (150 K) is somewhat lower for **3** than for **2**.

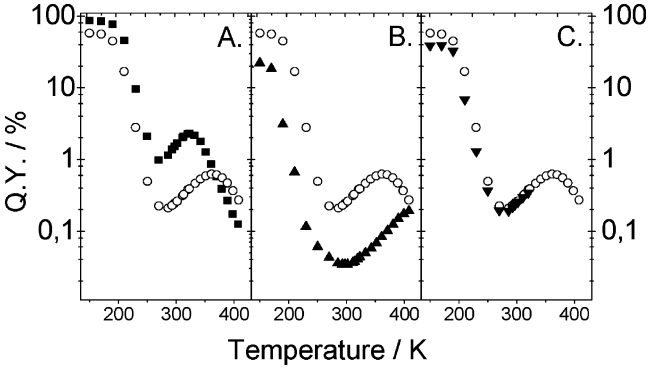

Figure 6. Temperature dependence (150 K < *T* < 410 K) of the emission quantum yield from **1** (filled squares) and **2** (open circles) in 1,2-propanediol (A), **2** in ethylene glycol (filled up-triangles) and **2** in 1,2-propanediol (open circles) (B), and **3** (filled down-triangles) and **2** (open circles) in 1,2-propanediol (C).

The normalized emission spectra in 1,2-propanediol glass at 150 K are compared in Figure 7. The spectra are progressively shifted to the red, and although their shapes are roughly the same, the vibrational bands are much better resolved for the rigid **3** compared to the other two complexes. The spacing

TABLE 3: Emission Properties of 1, 2, and 3 Bound to Poly(dAdT)$_2$

molecule	Φ[a] (%)	τ_1[b] (ns) (α_1)	τ_2[b] (ns) (α_2)	τ_{nat}[c] (μs)	λ_{em}[d] (nm)
Δ-**1**[e]	7.3	774 (0.59)	134 (0.41)	7.0	625
Λ-**1**[e]	1.4	310 (0.34)	42 (0.66)	9.5	625
ΔΔ-**2**	9.0	610 (0.63)	123 (0.37)	4.8	636
ΛΛ-**2**	1.1	124 (0.34)	45 (0.66)	6.5	684
ΔΔ-**3**	1.4	1267 (0.34)	213 (0.66)	40.8	640
ΛΛ-**3**	0.7	295 (0.60)	66 (0.40)	29.1	667

[a] Emission quantum yield. The quantum yields for **3** are calculated relative to the quantum yield for ΛΛ-**2**. [b] Emission lifetimes (τ) and, in parentheses, normalized preexponential factors reflecting mole fractions of the different luminescing species at $t = 0$. [c] τ_{nat} is calculated as $(\tau_1\alpha_1 + \tau_2\alpha_2)/\Phi$. [d] Wavelength of maximum emission. [e] Values from the literature.[6]

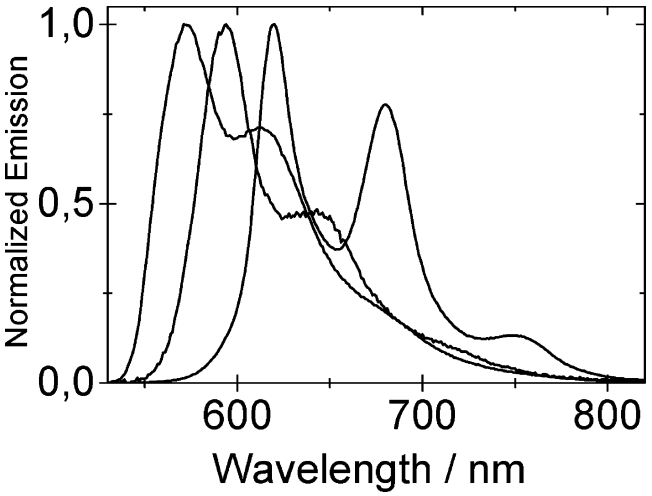

Figure 7. Normalized emission spectra of **1**, **2**, and **3** (from left to right) in 1,2-propanediol at 150 K.

between the vibrational peaks is 1140 cm^{-1} for **1**, 1280 cm^{-1} for **2**, and 1420 cm^{-1} for **3**.

Quantum yields, emission lifetimes, and emission maxima in the four solvents at room temperature are given in Table 4. As noted above, for a given solvent quantum yields for **2** and **3** are almost identical but several times lower than that for **1**. The natural lifetime increases in the order **1** < **2** < **3**, however, while it is essentially solvent independent for **1** and **2**, it increases with increasing quantum yield for **3**, being more than twice as long in 1,2-propanediol than in glycerol.

The effect from hydrogen bonding on the emission quantum yield of **2** was studied by using a method previously used to estimate the enthalpy of the solvent hydrogen bond formation to the MLCT excited state of **1**.[15,28] Assuming the emission spectral profiles of the differently hydrogen bonded species to be temperature and solvent independent, the emission spectra in 1,2-propanediol and ethylene glycol (above 300 K) could be uniquely resolved using singular value decomposition into two components corresponding to complex without (B) and with hydrogen bonds (C), respectively. A van't Hoff plot constructed from the natural logarithm of [B]/[C] versus inverse temperature (Figure 8) shows a linear region above 330 K with ΔH values characteristic of breaking strong solvent interactions (32 kJ/mol) in both solvents. Interestingly, these values are much larger than the 11−20 kJ/mol previously found for **1**,[28] explaining why the high-temperature emission quantum yield maximum occurs at a higher temperature for **2**.

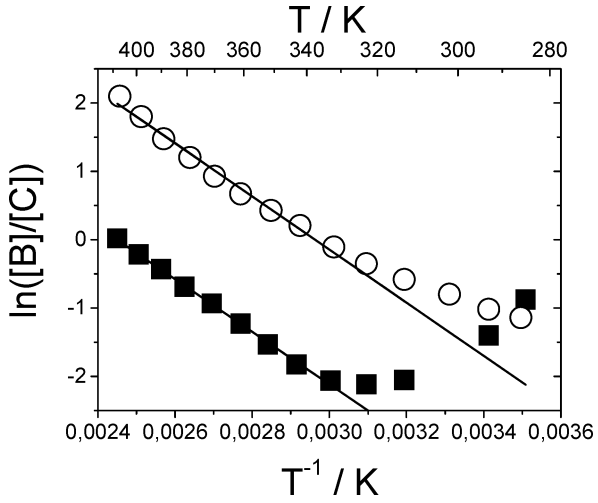

Figure 8. Natural logarithm ln([B]/[C]) plotted against inverse temperature (T^{-1}) for **2** in ethylene glycol (filled squares) and 1,2-propanediol (open circles). A straight line is fitted to the data for $T >$ 330 K (57 °C).

Discussion

The goal of this study has been to characterize in detail the DNA binding geometry of the flexible "light-switch" dimer [μ-bidppz(phen)$_4$Ru$_2$]$^{4+}$ (**2**) by comparing its DNA binding and its photophysical properties bound to DNA and in different hydrogen bonding solvents with those of the monomer [Ru(phen)$_2$dppz]$^{2+}$ (**1**) and a rigid homologue, [μ-dtpf-(phen)$_4$Ru$_2$]$^{4+}$ (**3**).

Conformation of 2 in Solution. That **2** has a twisted conformation in solution with a dihedral angle of approximately 40° between the planes of the two dppz units is supported by both the calculated energy minima for the bidppz ligand and the calculated and experimental transition energies compared to the planar dtpf ligand of the reference compound **3** (Table 1). It is, however, difficult to distinguish between the syn and anti rotamers, and free in solution there is most probably a 1:1 mixture of the two.

Binding of 3 to Poly(dAdT)$_2$. The gross similarity of the sluggish association and dissociation rates for **2** and **3**, as measured by luminescence, strongly supports that the binding of **3** also requires a major conformational change of the DNA in the rate-determining step, like the base pair opening proposed for the threading intercalation of **2**.[11,18] That the slow binding of **3** indeed is threading intercalation is shown by the LD spectra, in which the long-axis polarized $\pi-\pi^*$ transitions of the bridging dtpf ligand show strong negative LD bands, indicative

TABLE 4: Emission Properties for 1, 2, and 3 in Protic Solvents

molecule	solvent[a]	Φ[b] (%)	τ[c] (ns)	τ_{nat}[d] (μs)	λ_{em}[e] (nm)
1	Eg	0.070	6.9	9.9	658
2	Eg	0.034	4.3	12.6	722
3	Eg	0.029	7.9	27.2	733
1	Gly	0.14	7.3[f]	5.2	644
2	Gly	0.064	7.1[f]	11.1	700
3	Gly	0.055	12.5	22.7	727
1	1,2-pd	1.38	84.3	6.1	622
2	1,2-pd	0.23	29.0	12.6	687
3	1,2-pd	0.22	110.3	50.1	709
1	1,3-pd	0.41	26.8	6.5	631
2	1,3-pd	0.11	14.8	13.4	698
3	1,3-pd	0.11	48.3	43.9	717

[a] Solvents: ethylene glycol (Eg), glycerol (Gly), 1,2-propanediol (1,2-pd), and 1,3-propanediol (1,3-pd). [b] Emission quantum yields calculated relative to the quantum yield for **1** in glycerol in the literature.[28] [c] Emission lifetime (τ). [d] τ_{nat} is calculated as τ/Φ. [e] Wavelength of maximum emission. [f] Shorter lifetimes of 1.5 ns (**1**) and 4.4 (**2**) ns, respectively, contribute to the emission decay.

of a close to perpendicular orientation of this axis relative to the DNA helix, just as for **2**. It is interesting to note that, despite the total lack of conformational flexibility, **3** threads with rates similar to those of **2**, a rate of threading intercalation that is much slower than for the threading bis-intercalating complex $[\mu\text{-C4(cpdppz)}_2(\text{phen})_4\text{Ru}_2]^{4+}$,[29] a dimer of **1** in which the two dppz moieties are connected by a flexible chain. This shows that the rotational freedom around the biaryl bond of **2** is not enough to greatly facilitate the rate-determining threading step compared to **3**. On the contrary, while the association rates are found to be similar, the SDS-promoted dissociation of corresponding enantiomers is slower for **2** than for **3**, indicating that the threaded, intercalated binding mode is thermodynamically less favorable for **3**, and that its locked planar syn conformation may not give an optimal fit to the binding site. Although this observation has to be interpreted with some caution, since the DNA dissociation rates obtained with the SDS sequestration technique may be significantly catalyzed by the detergent,[30,31] the spectroscopic evidence is clearly in favor of a preferred nonplanar conformation of intercalated **2** as discussed below.

DNA Binding Geometry of 2 and 3. That **2** is not planar when intercalated into DNA, as suggested by the previous LD study on the ΔΔ, ΛΛ, and ΔΛ (meso) stereoisomers[17] and the thermodynamic considerations above, is further supported by comparison of red shift and hypochromic effect on DNA binding with the planar **3** (Table 2). The earlier study suggested further that **2** binds in its anti conformation, based on comparison of the strong induced CD upon DNA binding with a calculation of the Cotton effect for a twisted bidppz ligand.[17] This argument fails, though, since the present results show that the CD induced by DNA binding primarily is due to coupled oscillator interactions of the bridging ligand with the DNA bases, as the induced CD is of very similar amplitude and sign for the chiral twisted bidppz of **2** and the planar, achiral dtpf of **3** (Figure 3). Thus, since the CD originating from the twisted, intrinsically chiral bidppz chromophore apparently is too weak to be reliably determined, we cannot from the induced CD of **2** bound to DNA deduce whether the conformation is syn or anti. However, although the totally planar conformation may be thermodynamically unfavorable, a syn conformation is clearly possible to accommodate in the intercalation pocket, and the close similarities between the corresponding enantiomers of **2** and **3** in the induced CD, in LD, and in threading kinetics indicate that **2** actually binds in a similar, but twisted, conformation as **3**, i.e., as a syn rotamer rather than as an anti rotamer.

Analysis of the LD spectra for **2** and **3** bound to poly(dAdT)$_2$ provides further details of the binding geometries. Below 300 nm the spectra are dominated by the long-axis polarized $\pi \rightarrow \pi^*$ transitions of the phenanthroline ligands, overlaid with the negative polynucleotide band at 260 nm. For the monomer **1**, we have shown that the difference between the Δ-enantiomer (strongly positive phenanthroline LD) and Λ-enantiomer (weakly positive or zero phenanthroline LD) is due to a clockwise roll around the dppz long axis of approximately 10°, for both the Δ-enantiomer and the Λ-enantiomer. This common deviation from an idealized B-DNA intercalation geometry will rotate the phenanthroline transitions to be more parallel to the helix axis for the Δ-enantiomer but to be more perpendicular for the Λ-enantiomer, leading to the observed LD differences.[7,32] In our previous study on the stereoisomers of **2**, similar differences in the LD spectra in the <300 nm region were interpreted as being consistent with an analogous binding geometry, in which, for all three stereoisomers, one of the $[\text{Ru(phen)}_2\text{dppz}]^{2+}$ subunits of **2** is deeply intercalated with a clockwise roll angle, and the other subunit, twisted in the positive sense around the biaryl bond, protrudes into the opposite groove.[17] Here we note that for **3**, which does not deviate much from a structure of D_2 symmetry, a common roll angle, for both enantiomers, of one Ru(phen)_2dppz subunit will effectively rotate the other subunit in the opposite sense and hence largely cancel the effect on the phenanthroline LD. Thus, for **3** we must allow different roll angles for the two enantiomers. A rotation around the 2-fold symmetry axis of **3** will differentiate most effectively the LD of the phenanthrolines, but at the same time also the LD of the strong long-axis polarized dtpf transitions. In fact, we observe weaker LD bands for these transitions for the ΛΛ-enantiomer. Assuming the same orientation factor S for both enantiomers, their LD spectra can be qualitatively described by the following binding geometries: for ΔΔ-**3**, the plane of the dtpf ligand is assumed perpendicular to the helix axis; for ΛΛ-**3**, the plane is tilted by a rotation of 30° around the 2-fold axis in an anticlockwise sense when regarded from the methylene group of the five-membered ring. Given the overall similarities of the LD spectra of corresponding enantiomers of **2** and **3**, an analogous explanation of the LD data for **2** is possible, in which different roll angles for the ΔΔ-, ΛΛ-, and ΔΛ-stereoisomers contribute to the differences in the LD of the phenanthroline band. However, since **2** is twisted, the sense of the twist will nevertheless have a major influence on the phenanthroline LD, and our earlier conclusion about a positive twist sense still remains valid.

Photophysical Properties in Protic Solvents. The emission quantum yields of the two binuclear complexes **2** and **3** are lower than that of **1** at all temperatures in all solvents studied. A decreased quantum yield is probably related to a smaller separation of the excited state and the ground state as a result of the larger conjugated aromatic systems, which is also evident by the wavelength of maximum emission, where the binuclear complexes emit light at longer wavelengths. The increase in natural lifetime from **1** to **3** also parallels the increase in the degree of conjugation, and may reflect that the radiative rate constant of a more delocalized charge-separated state on a large aromatic ligand is less influenced by the spin−orbit coupling of the heavy ruthenium ion. However, the observation that introduction of a methyl substituent at C10 (but not at C11 and C12) of the dppz moiety of **1** also leads to increased natural lifetimes[28] indicates that the photophysical properties also sensitively depend on other factors, including electronic and solvent perturbations.

The emission quantum yield of **2** increases significantly in a temperature range immediately above 300 K, in contrast to a general decrease below 300 K. This is because the equilibrium between unquenched, non-hydrogen-bonded (B) and quenched, hydrogen-bonded (C) excited-state species is shifted toward non-hydrogen-bonded species at higher temperatures.

The enthalpy difference between the C and B species is estimated to be significantly larger for **2** compared to **1**, making its quantum yield more sensitive to solvent hydrogen bonding. This may simply be due to the double number of nitrogens that can be hydrogen bonded in **2**, but may also reflect stronger solvent interactions due to a more efficient charge separation with the larger π-system of the bidppz ligand.

At higher temperatures the emission quantum yield decreases again with temperature, now due to thermal population of a nonradiative metal centered state, as can be seen by that the temperature dependence in this region is similar to that found for **1** and $[\text{Ru(phen)}_3]^{2+}$.

Photophysical Properties When Bound to DNA. Studying the emission quantum yield for the enantiomers of the binuclear complexes bound to DNA reveals that ΔΔ-**2** stands out by having a much higher quantum yield, in particular compared to ΔΔ-**3**, when bound to poly(dAdT)$_2$ despite the small differences between **2** and **3** in the protic solvents. The quantum yield and the emission lifetimes are similar when comparing ΔΔ-**2** and Δ-**1** bound to poly(dAdT)$_2$. However, since **2** appears more efficiently quenched by solvent hydrogen bonding than **1**, this seems to suggest that ΔΔ-**2** binds to poly(dAdT)$_2$ in a way that gains extra protection from quenching by water. However, the natural lifetime for both enantiomers of **2** is much lower when bound to DNA than in the polyol solvents. As argued above, this observation may be explained by a charge transfer that is essentially localized to the deeply intercalated Ru(phen)$_2$dppz moiety, making the influence of the spin−orbit coupling with the heavy ruthenium nucleus more pronounced. Thus, the water quenching characteristics of **2** when intercalated into DNA may in fact be closer to those of **1** free in solution than to **2**, suggesting that the water accessibility to the deeply intercalated dppz moiety of ΔΔ-**2** could indeed be quite similar to that of Δ-**1**.

Conclusions

By comparing the semiflexible binuclear complex **2** with its rigid, planar homologue **3** and the parent "light-switch" complex **1**, when bound to poly(dAdT)$_2$ or free in solution, several conclusions about DNA binding geometry and photophysical properties can be drawn:

(i) Both enantiomers of **3**, which can be regarded as a planar syn rotamer of **2**, can intercalate into poly(dAdT)$_2$ with overall binding geometries similar to those of corresponding enantiomers of **2**.

(ii) **2** is significantly twisted, both free in solution and intercalated into DNA, with a dihedral angle between the molecular planes of the dppz moieties of roughly 40° or 140°.

(iii) The induced CD of **2** mainly originates from a coupled oscillator mechanism between the nucleobases and the bridging ligand, and not from the chiral, twisted conformation of the latter, which means that we cannot distinguish between 40° (syn) and 140° (anti) twist.

(iv) Polyol solvents are more strongly hydrogen bonded to the excited state of **2** than to **1**.

(v) For **2**, the radiative rate constant increases to a value similar to that for **1** on intercalation into DNA, which suggests that the MLCT excited states of **1** and **2** may accept hydrogen bonds equally well when intercalated, leading to the conclusion that their Δ-enantiomers are similarly protected from water in DNA.

Supporting Information Available: Calculated rotational barrier for the bridging ligand. CD spectra of the enantiomers of **2** and **3** in water and bound to poly(dAdT)$_2$. Temperature dependence for the emission quantum yield of **1**, **2**, and **3** in glycerol, ethylene glycol, 1,3-propanediol, and 1,2-propanediol. Emission spectra of **1**, **2**, and **3** at 230, 210, 190, 170, and 150 K. Relative concentration of species B and C of **2** in 1,2-propanediol. Normalized emission spectra of species B and C of **2** in 1,2-propanediol and ethylene glycol. This material is available free of charge via the Internet at http://pubs.acs.org.

References and Notes

(1) Barton, J. K.; Danishefsky, A.; Goldberg, J. *J. Am. Chem. Soc.* **1984**, *106* (7), 2172−2176.

(2) Barton, J. K.; Goldberg, J. M.; Kumar, C. V.; Turro, N. J. *J. Am. Chem. Soc.* **1986**, *108* (8), 2081−2088.

(3) Pyle, A. M.; Barton, J. K. *Prog. Inorg. Chem.* **1990**, *38*, 413−475.

(4) Friedman, A. E.; Chambron, J. C.; Sauvage, J. P.; Turro, N. J.; Barton, J. K. *J. Am. Chem. Soc.* **1990**, *112* (12), 4960−4962.

(5) Chow, C. S.; Barton, J. K. *Methods Enzymol.* **1992**, *212*, 219−242.

(6) Hiort, C.; Lincoln, P.; Nordén, B. *J. Am. Chem. Soc.* **1993**, *115* (9), 3448−3454.

(7) Lincoln, P.; Broo, A.; Nordén, B. *J. Am. Chem. Soc.* **1996**, *118* (11), 2644−2653.

(8) Nordén, B.; Lincoln, P.; Åkerman, B.; Tuite, E. *Met. Ions Biol. Syst.* **1996**, *33*, 177−252.

(9) Erkkila, K. E.; Odom, D. T.; Barton, J. K. *Chem. Rev. (Washington, D.C.)* **1999**, *99* (9), 2777−2795.

(10) Önfelt, B.; Lincoln, P.; Nordén, B. *J. Am. Chem. Soc.* **1999**, *121* (46), 10846−10847.

(11) Wilhelmsson, L. M.; Westerlund, F.; Lincoln, P.; Nordén, B. *J. Am. Chem. Soc.* **2002**, *124* (41), 12092−12093.

(12) Westerlund, F.; Pierard, F.; Eng, M. P.; Norden, B.; Lincoln, P. *J. Phys. Chem. B* **2005**, *109* (36), 17327−17332.

(13) Olson, E. J. C.; Hu, D.; Hoermann, A.; Jonkman, A. M.; Arkin, M. R.; Stemp, E. D. A.; Barton, J. K.; Barbara, P. F. *J. Am. Chem. Soc.* **1997**, *119* (47), 11458−11467.

(14) Coates, C. G.; Olofsson, J.; Coletti, M.; McGarvey, J. J.; Oenfelt, B.; Lincoln, P.; Norden, B.; Tuite, E.; Matousek, P.; Parker, A. W. *J. Phys. Chem. B* **2001**, *105* (50), 12653−12664.

(15) Olofsson, J.; Önfelt, B.; Lincoln, P. *J. Phys. Chem. A* **2004**, *108* (20), 4391−4398.

(16) Lincoln, P.; Nordén, B. *Chem. Commun.* **1996**, (18), 2145−2146.

(17) Wilhelmsson, L. M.; Esbjörner, E. K.; Westerlund, F.; Norden, B.; Lincoln, P. *J. Phys. Chem. B* **2003**, *107* (42), 11784−11793.

(18) Nordell, P.; Lincoln, P. *J. Am. Chem. Soc.* **2005**, *127* (27), 9670−9671.

(19) Westerlund, F.; Wilhelmsson, L. M.; Norden, B.; Lincoln, P. *J. Phys. Chem. B* **2005**, *109* (44), 21140−21144.

(20) Krausz, E.; Ferguson, J. *Prog. Inorg. Chem.* **1989**, *37*, 293−390.

(21) Chambron, J. C.; Sauvage, J. P.; Amouyal, E.; Koffi, P. *Nouv. J. Chim.* **1985**, *9* (8−9), 527−529.

(22) Önfelt, B.; Olofsson, J.; Lincoln, P.; Nordén, B. *J. Phys. Chem. A* **2003**, *107* (7), 1000−1009.

(23) Tuite, E.; Lincoln, P.; Nordén, B. *J. Am. Chem. Soc.* **1997**, *119* (1), 239−240.

(24) Barker, A.; Barker, C. C. *J. Chem. Soc.* **1954**, 1307−1309.

(25) Lefevre, R. J. W.; Moir, D. D.; Turner, E. E. *J. Chem. Soc.* **1927**, 2330−2339.

(26) Nordén, B.; Kubista, M.; Kurucsev, T. *Q. Rev. Biophys.* **1992**, *25* (1), 51−170.

(27) Frisch, M. J.; Trucks, G. W.; Schlegel, H. B.; Scuseria, G. E.; Robb, M. A.; Cheeseman, J. R.; Montgomery, J. A., Jr.; Vreven, T.; Kudin, K. N.; Burant, J. C.; Millam, J. M.; Iyengar, S. S.; Tomasi, J.; Barone, V.; Mennucci, B.; Cossi, M.; Scalmani, G.; Rega, N.; Petersson, G. A.; Nakatsuji, H.; Hada, M.; Ehara, M.; Toyota, K.; Fukuda, R.; Hasegawa, J.; Ishida, M.; Nakajima, T.; Honda, Y.; Kitao, O.; Nakai, H.; Klene, M.; Li, X.; Knox, J. E.; Hratchian, H. P.; Cross, J. B.; Adamo, C.; Jaramillo, J.; Gomperts, R.; Stratmann, R. E.; Yazyev, O.; Austin, A. J.; Cammi, R.; Pomelli, C.; Ochterski, J. W.; Ayala, P. Y.; Morokuma, K.; Voth, G. A.; Salvador, P.; Dannenberg, J. J.; Zakrzewski, V. G.; Dapprich, S.; Daniels, A. D.; Strain, M. C.; Farkas, O.; Malick, D. K.; Rabuck, A. D.; Raghavachari, K.; Foresman, J. B.; Ortiz, J. V.; Cui, Q.; Baboul, A. G.; Clifford, S.; Cioslowski, J.; Stefanov, B. B.; Liu, G.; Liashenko, A.; Piskorz, P.; Komaromi, I.; Martin, R. L.; Fox, D. J.; Keith, T.; Al-Laham, M. A.; Peng, C. Y.; Nanayakkara, A.; Challacombe, M.; Gill, P. M. W.; Johnson, B.; Chen, W.; Wong, M. W.; Gonzalez, C.; Pople, J. A. *Gaussian 03*, revision B.05; Gaussian, Inc.: Pittsburgh, PA, 2003.

(28) Olofsson, J.; Wilhelmsson, L. M.; Lincoln, P. *J. Am. Chem. Soc.* **2004**, *126* (47), 15458−15465.

(29) Önfelt, B.; Lincoln, P.; Nordén, B. *J. Am. Chem. Soc.* **2001**, *123* (16), 3630−3637.

(30) Westerlund, F.; Wilhelmsson, L. M.; Norden, B.; Lincoln, P. *J. Am. Chem. Soc.* **2003**, *125* (13), 3773−3779.

(31) Marcus, R. A. *J. Phys. Chem. B* **2005**, *109* (45), 21419−21424.

(32) Lincoln, P.; Nordén, B. *J. Phys. Chem. B* **1998**, *102* (47), 9583−9594.